Journal of Alloys and Compounds 488 (2009) 57–64

Contents lists available at ScienceDirect

Journal of Alloys and Compounds

journal homepage: www.elsevier.com/locate/jallcom

Microstructure and mechanical property of as-cast, -homogenized, and -deformed $Al_xCoCrFeNi$ ($0 \le x \le 2$) high-entropy alloys

Yih-Farn Kao [a], Ting-Jie Chen [a], Swe-Kai Chen [b,*], Jien-Wei Yeh [a]

[a] Department of Materials Science and Engineering, National Tsing Hua University, 101 Kuang Fu Road, Sec. 2, Hsinchu 30013, Taiwan, ROC
[b] Center for Nanotechnology, Materials Science and Microsystems, National Tsing Hua University, 101 Kuang Fu Road, Sec. 2, Hsinchu 30013, Taiwan, ROC

ARTICLE INFO

Article history:
Received 26 July 2009
Received in revised form 19 August 2009
Accepted 19 August 2009
Available online 27 August 2009

Keywords:
Metals and alloys
Microstructure
Scanning electron microscopy
SEM
X-ray diffraction

ABSTRACT

To have a further investigation of their physical properties such as electrical, magnetic, and thermal properties, the microstructure and mechanical property of $Al_xCoCrFeNi$ alloys have to have a detailed and systematic study. We present the effects of Al content on microstructure and mechanical property of as-cast, -homogenized, and -deformed $Al_xCoCrFeNi$ alloys in this study. It shows that single FCC and single BCC solutions, and duplex FCC–BCC are principal phases in these alloys. The x intervals for duplex FCC–BCC of different states of these alloys are investigated. The spinodal decomposition of less Al–Ni and more Al–Ni phases is the major reaction during homogenization of the alloys. The morphology of the less and more Al–Ni phases is also discussed. There is no stress-induced phase transformation during 50%-rolling deformation, and the main strengthening mechanism is work hardening. The hardening ability of FCC was about twice that of BCC in this alloy system.

1. Introduction

The conventional strategy for developing alloys has selected one or two principal components for primary properties and other minor components for acquisition of definite microstructure and properties, such as steels, Ti–Al intermetallics [1], bulk metallic glasses [2–4], etc. Traditional metallurgical theory suggests that multiple alloying elements in an alloy lead to the formation of many compounds with complex microstructure and poor mechanical properties [5]. However, recently this paradigm has been broken by new alloy system, high-entropy alloys (HEAs). The HEAs were suggested by Professor Jien-Wei Yeh and demonstrated by Professor Swe-Kai Chen, respectively, at the National Tsing Hua University in 1995 [6]. HEA greatly differs from conventional alloys because multiple major components are used in the former rather than only one or two component(s) in the latter. Moreover, HEA is defined as an alloy containing n major elements, where n is between 5 and 13, and the molar ratio of each element is from 5 to 35 at%. The selection of HEA certainly causes new findings, so HEA is expected to develop more alloys that have special properties.

HEA has been studied extensively in recent years, and has more excellent properties than conventional alloys: high ability of forming nano-scale precipitation [7], good thermal stability [8], superior extensive or compressive [9] properties, extremely high hardness [8], excellent anticorrosive properties [10], special electrical and magnetic properties [11], and simple microstructures with solid solution of multiple elements [12–14]. Great applications [15–23], such as molds and structural materials at high temperature, wearing and abrasion-resistant coating, and even military engineering, have generally been expected in terms of the above unique characteristics. Consequently, not only large applied advantages but also great investigation potential indeed exists in HEAs.

Kinds of alloys like $Al_xCoCrFeNi$ have been the most thoroughly studied high-entropy alloys until now. However, properties such as electrical, magnetic, and thermal of these alloys are of research interest. Therefore, in this study, effects of various Al contents in $Al_xCoCrFeNi$ (x = 0–2) on the hardness and microstructure will be discussed from their as-cast, -homogenized, and -deformed states by XRD, SEM/EDS, and Vickers hardness tester. The relation of hardness to microstructure is also quantitatively discussed. It is aimed to provide a reference study for further physical investigations discussed elsewhere. Therefore, basic data such as the lattice constants of different processing conditions are also listed in this study.

2. Experimental details

Al, Co, Cr, Fe, and Ni with purity greater than 99.5% are used. A total of 40–50 g material was used to prepared $Al_xCoCrFeNi$ ($0 \le x \le 2$) alloys by vacuum arc-remelter. After the alloys were re-melted, they were turned over for process repeating at least three times to insure that the alloys were well mixed. As-cast alloys were heated to 1100 °C at a rate of 20 °C/min and stayed at 1100 °C for 24 h. The samples were then water quenched. These heated and quenched samples are called as-homogenized ones. The homogenized samples were cold deformed by the DBR250 two-high rolling mill to a 50% reduction of thickness. Cracks appeared for

* Corresponding author. Tel.: +886 3 574 2569; fax: +886 3 571 3113.
E-mail address: skchen@mx.nthu.edu.tw (S.-K. Chen).

0925-8388/$ – see front matter © 2009 Elsevier B.V. All rights reserved.
doi:10.1016/j.jallcom.2009.08.090

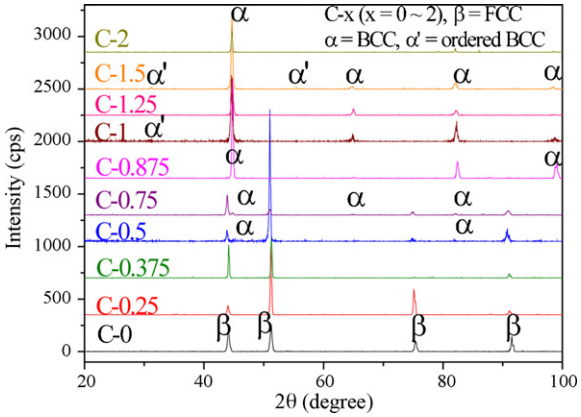

Fig. 1. XRD patterns for C-x ($0 \le x \le 2$) showing the phase change from FCC to BCC as x increases.

samples with the molar ratio of Al over 0.875 (i.e., $x > 0.875$) owing to the high hardness of the samples. Therefore the as-deformed samples are only for $0 \le x \le 0.875$ in this study. Hereafter C-x, H-x, and D-x represent as-cast, -homogenized, and -deformed $Al_xCoCrFeNi$ ($0 \le x \le 2$) alloys, respectively. Before microstructural observation, the as-cast, -homogenized, and -deformed samples were cut with diamond cutter, and ground by #240, #400, #800, #1200, #2000, #2400, and #4000 SiC sandpapers in sequence. The samples were then wet-polished with 1, 0.3, and 0.05 μm Al_2O_3 powders. A JEOL JSM840A SEM was used to observe the microstructure of the samples, and composition was analyzed with energy dispersive X-ray spectroscopy (EDS). An X-ray diffractometer RIGAKU ME510-FM2 was employed to test the crystal structure of the samples. The Cu target whose characteristic wavelength $\lambda(K\alpha_1) = 1.54056$ Å was used, and the working voltage and current were 30 kV and 20 mA, respectively. The scanning range 2θ was from 20° to 100°, and the scanning rate was 4°/min. The lattice constants were obtained by the standard procedure introduced in usual textbook [24]. The hardness was measured with a hardness tester, MATSUZAWA SEIKI MV-1. The samples were imposed load of 5 kg, load time of 15 s, and load rate of 50 μm/s. Each sample was measured at seven distinct regions and the average of the values was taken as the hardness value.

3. Results and discussion

3.1. As-cast $Al_xCoCrFeNi$ (C-x)

According to the XRD patterns shown in Fig. 1 and SEM images shown in Fig. 2, the microstructure for C-0, C-0.25, and C-0.375 is single face-centered cubic (FCC) phase. The microstructure for C-0.50 and C-0.75 is body-centered cubic (BCC) and FCC duplex phase (Figs. 1 and 2(c)–(e)). The microstructure for C-0.875 to C-2.00 becomes single BCC phase as shown in Figs. 1 and 2(f)–(j). Interestingly, grain structures are observed in Fig. 2(h)–(j). The compositional analyses by EDS on different phases obtained from Fig. 2 are listed in Table 1. Lattice constants for C-x alloys are listed in Table 2. From the above discussion, one can draw a conclusion that Al is a BCC former. This conclusion conforms to the same results of Refs. [8,25]. As the amount of Al increases ($x \ge 1$), one can also observe the ordered BCC peaks (Fig. 1). Note that, in Fig. 1, the 3rd peak of FCC (2 2 0), in C-0.375 and the 2nd peak of BCC (2 0 0), in C-0.875 are missing.

The hardness for C-x alloys is listed in Table 2 and illustrated in Fig. 3. Note that both C-0.375 and C-0.875 alloys have the high-

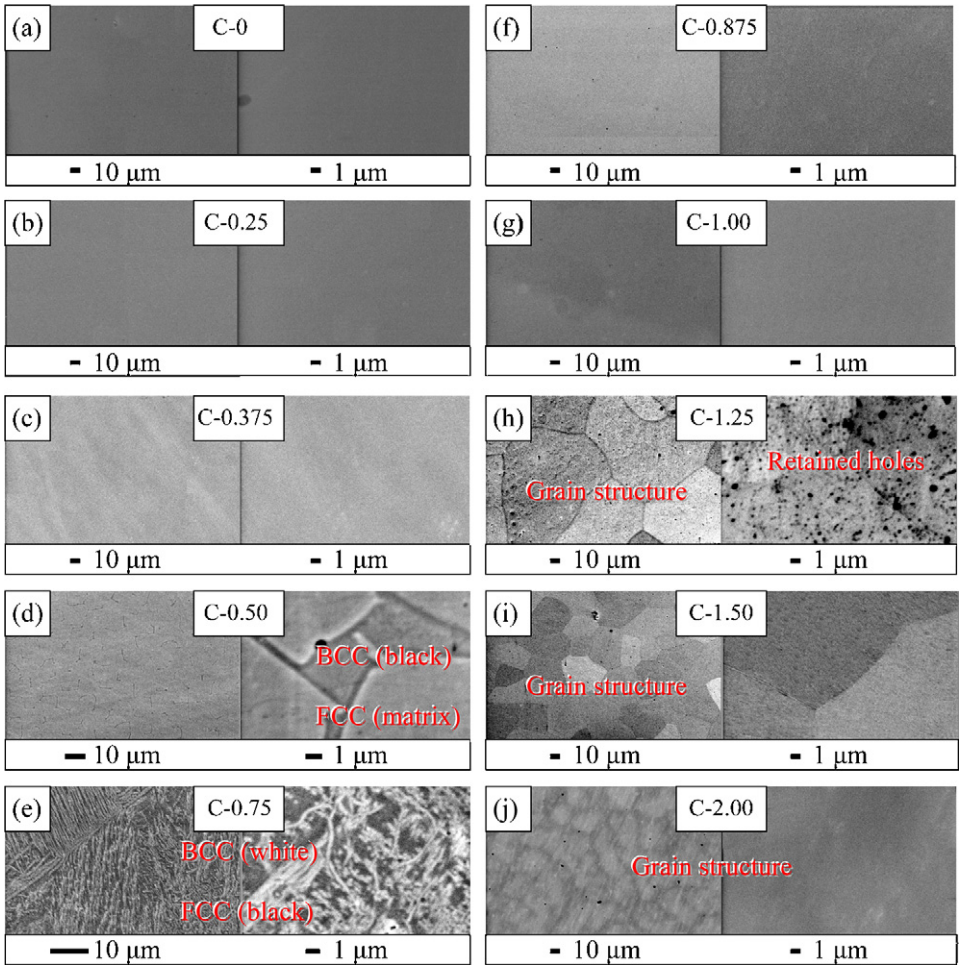

Fig. 2. SEM images for not etched C-x samples with lower (left) and higher (right) magnifications.

Table 1
EDS analyses (at%) for C-*x*.[a]

Samples	Items	Al (%)	Co (%)	Cr (%)	Fe (%)	Ni (%)
C-0	Designed	0	25.00	25.00	25.00	25.00
	Overall (FCC)	0	24.16	26.82	24.48	24.66
C-0.25	Designed	5.88	23.53	23.53	23.53	23.53
	Overall (FCC)	5.61	23.14	24.58	24.10	22.58
C-0.375	Designed	8.57	22.86	22.86	22.86	22.86
	Overall (FCC)	7.82	22.61	23.68	23.34	22.55
C-0.50[b]	Designed	11.11	22.22	22.22	22.22	22.22
	Overall	12.4	21.02	22.80	20.91	22.87
	FCC (87.83%)	10.36	21.80	23.50	21.83	22.52
	BCC (12.16%)	16.93	18.65	24.07	18.50	21.86
C-0.75[b]	Designed	15.79	21.05	21.05	21.05	21.05
	Overall	15.00	21.04	22.29	21.16	20.51
	FCC (27.28%)	13.19	21.60	23.89	22.43	18.88
	BCC (72.72%)	15.86	20.99	22.27	20.80	22.07
C-0.875	Designed	17.95	20.51	20.51	20.51	20.51
	Overall (BCC)	16.18	20.56	21.83	21.33	20.10
C-1.00	Designed	20.00	20.00	20.00	20.00	20.00
	Overall (BCC)	18.26	19.78	21.12	20.68	20.17
C-1.25	Designed	23.81	19.05	19.05	19.05	19.05
	Overall (BCC)	23.03	19.36	19.28	18.74	19.59
C-1.50	Designed	27.27	18.18	18.18	18.18	18.18
	Overall (BCC)	27.79	18.17	18.30	18.08	17.66
C-2.00	Designed	33.33	16.67	16.67	16.67	16.67
	Overall (BCC)	32.01	16.79	17.60	16.78	16.81

[a] Volume fractions in duplex region are shown. "Designed" means the designed compositions. The volume fractions of FCC and BCC phases in the transition region calculated by hardness information shown in Fig. 3 and by Eq. (1).
[b] Shows the FCC–BCC transition region.

Table 2
Lattice constants and hardness of C-*x*.

Sample	Lattice constant (Å)		Hardness (Hv)
	FCC phase	BCC phase	
C-0	3.559	–	116.0 ± 3
C-0.25	3.567	–	110.0 ± 2
C-0.375	3.560	–	130.8 ± 0.5
C-0.50[a]	3.574	2.854	159.0 ± 2
C-0.75[a]	3.569	2.861	388.0 ± 5
C-0.875	–	2.860	538.0 ± 12
C-1.00	–	2.869	484.0 ± 26
C-1.25	–	2.860	487.0 ± 19
C-1.50	–	2.866	484.0 ± 5
C-2.00	–	2.867	509.0 ± 27

[a] Shows the FCC–BCC transition region.

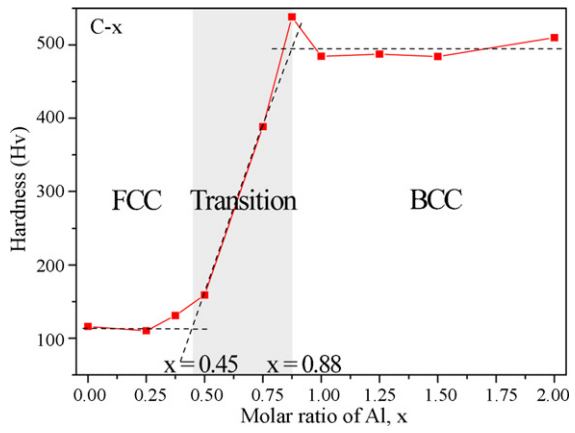

Fig. 3. Hardness of C-*x* vs. *x* plot with the schematic plot (dashed line) for determining the boundaries of the transition region in C-*x*.

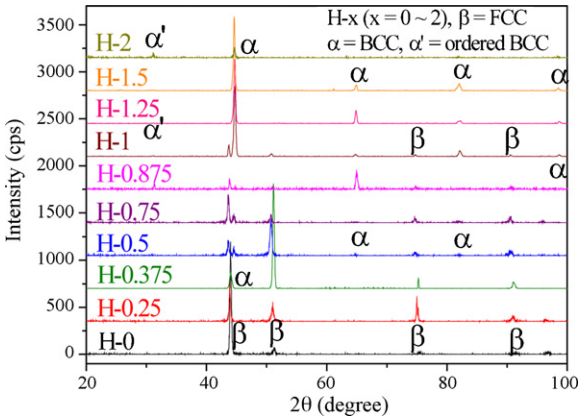

Fig. 4. The XRD patterns for not etched H-*x* ($0 \le x \le 2$) showing the phase change from FCC to BCC as *x* increases.

est hardness for single FCC or single BCC phase in C-*x* alloys, respectively. This can be attributed to the supersaturated solution hardening and the texture mentioned in the last paragraph. The phases of C-0.375 and C-0.875 are not thermodynamically stable because they were fast cooled during casting. Hence, the atoms did not have enough time to accommodate themselves or to combine to form a new phase. This result was moreover confirmed after homogenization (mentioned in the next section).

According to Fig. 3, the phase can be divided into three regions. That is (1) FCC for $0 \le x \le 0.375$, (2) FCC–BCC for $0.50 \le x \le 0.75$, and (3) BCC for $0.875 \le x \le 2.00$ for C-*x* alloys. Two vertical lines are aligned to the average hardness lines of FCC and BCC and intersected the inclined line of the FCC–BCC transition region as shown in Fig. 3. The intersecting points thus made correspond to the boundaries of the transition region and they are approximately $x = 0.45$ and 0.875. However, the boundaries are relatively unstable (see below for further discussion). The volume fractions of FCC and BCC phase in the transition region can be calculated as follows. The average hardness values of single FCC and single BCC are designated to be H_{FCC} and H_{BCC}, respectively. Accordingly, the hardness *H* in the transition region can be expressed as follows:

$$H = aH_{FCC} + (1-a)H_{BCC}, \quad a = \frac{(H_{BCC} - H)}{(H_{BCC} - H_{FCC})}, \tag{1}$$

where *a* is the volume fraction of FCC, and $(1-a)$ is that of BCC. By doing this, one can obtain the *x* interval for transition region of C-*x* to be as $0.45 \le x \le 0.88$, rather than to be as $0.50 \le x \le 0.75$. Hence, the volume fraction for C-*x* can be shown in Table 1. The later sections also use this method to determine the detailed transition boundaries and the volume fractions of FCC and BCC in various conditions. This calculation is helpful for discussion, especially in resistivity and magnetic properties that depend sensitively on microstructure.

3.2. As-homogenized $Al_xCoCrFeNi$ (H-*x*)

There is phase change for as-cast $Al_xCoCrFeNi$ after homogenization 24 h at 1100 °C. XRD patterns, SEM images, and hardness-*x* plot for H-*x* are shown in Figs. 4–6, respectively. The black spots shown at the right side of Fig. 5(g) are retained holes formed during casting. Composition from EDS, and lattice constants and hardness for H-*x* are listed in Tables 3 and 4, respectively. One can easily see that Al–Ni-rich BCC phase appears for alloys of $x \ge 0.375$. Although XRD patterns show single BCC phase for $x \ge 1.25$, there are still Al–Ni-rich phases for $x \ge 0.375$ in structure as can be seen in Fig. 5(c)–(g) and Table 3. It suggests, in this study, that the Al–Ni-rich phase appears as a result of relatively large mixing enthalpy

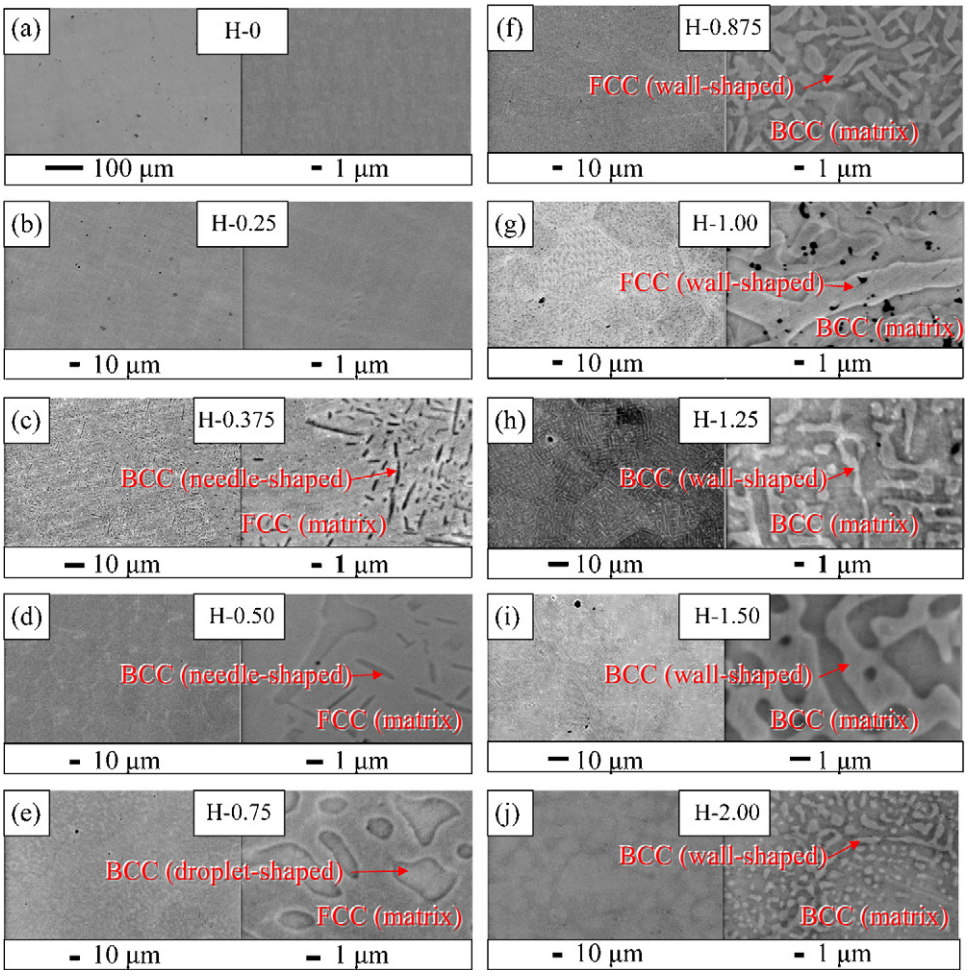

Fig. 5. SEM images for H-*x* samples with lower (left) and higher (right) magnifications.

between Al and Ni. That is, for $0.375 \le x \le 1.00$ there is Al–Ni-rich phase, which is an ordered BCC phase. For $1.25 \le x \le 2.00$, in addition to the formation of ordered BCC Al–Ni-rich matrix phase, there is an Al–Ni-less BCC phase. After homogenization, the Al–Ni-rich phase coarsens as can be seen in Fig. 5(d)–(e) for H-0.50 and H-0.75. The Al–Ni-rich phase can have various kinds of morphology from needle- (for H-0.375 and H-0.50) to droplet-shaped (for H-0.75). The Al–Ni-rich phase becomes matrix phase for H-0.875 to H-2.00, and the Al–Ni-less phase is wall-shaped. One can see that the FCC phase is also wall-shaped for H-0.875 and H-1.00 (Fig. 5). The wall-shaped microstructure from H-0.875 to H-2.00 might be from spinodal decomposition similar to the appearance of Al–Ni-rich phase in Alnico alloys [26]. Therefore, Al–Ni-rich phase in this study is probably from spinodal decomposition rather than the process of nucleation and growth. The Al–Ni-rich phase actually has an ordered CsCl structure corresponding to the peak of ordered BCC in Fig. 4. Comparing with Fig. 3, the hardness of H-*x* listed in Table 4 and shown in Fig. 6 (referred to the dashed schematic line) also agreed that the hardness increases due to increase in volume fraction of BCC phase for H-0.375 and H-0.50. On the contrary, the hardness decreases due to decrease in volume fraction of BCC phase for H-0.75, H-0.875, and H-1.00. The values of hardness of single FCC and single BCC phases are about 110 and 500 Hv, respectively, and are almost identical in both C-*x* and H-*x*. This implies that the hardness of Al–Ni-rich phase in H-0.375 to H-0.75 are similar to that of the BCC matrix phase in H-0.875 to H-2.00.

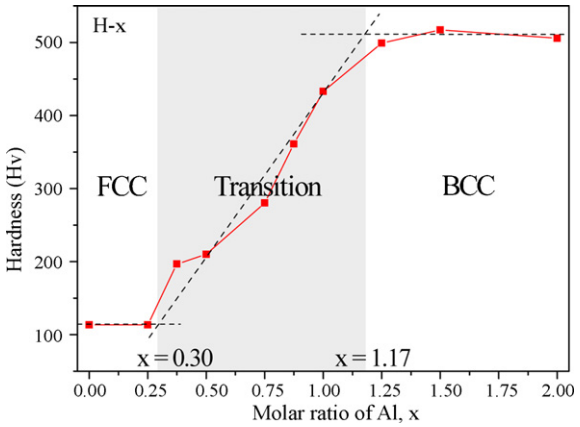

Fig. 6. Hardness of H-*x* vs. *x* plot and the schematic plot (dashed line) for determining the boundaries of the transition region in H-*x*.

By the same method discussed in the previous section and according to Eq. (1), the boundaries of the transition region and the volume fractions of FCC and BCC can be calculated and shown in Fig. 6 and listed in Table 3. The *x* interval of the transition region for H-*x* thus calculated is $0.30 \le x \le 1.17$, which is very near the interval of $0.375 \le x \le 1.00$ discussed above from the microstructure study. In addition, it is observed for the transition region that the volume fraction of BCC phase is roughly proportional to the molar ratio of Al to the power of 3 and proportional to the atomic percent of Al to

Table 3
EDS analyses (at%) for H-*x*.[a]

Samples	Items	Al (%)	Co (%)	Cr (%)	Fe (%)	Ni (%)
H-0	Designed	0	25.00	25.00	25.00	25.00
	Overall (FCC)	0	24.47	26.05	25.09	24.40
H-0.25	Designed	5.88	23.53	23.53	23.53	23.53
	Overall (FCC)	5.89	23.21	24.49	23.82	22.59
H-0.375[b]	Designed	8.57	22.86	22.86	22.86	22.86
	Overall	8.03	22.63	23.44	23.22	22.69
	FCC (78.85%)	6.20	23.34	24.75	24.19	21.52
	N-BCC (21.15%)	15.78	19.88	18.10	19.14	27.1
H-0.50[b]	Designed	11.11	22.22	22.22	22.22	22.22
	Overall	12.10	22.63	21.55	21.66	22.06
	FCC (75.51%)	7.81	22.90	25.24	24.02	20.03
	N-BCC (24.49%)	29.51	16.42	9.44	12.04	32.60
H-0.75[b]	Designed	15.79	21.05	21.05	21.05	21.05
	Overall	15.66	21.19	21.54	20.92	20.69
	FCC (57.65%)	7.84	22.68	27.77	25.61	16.1
	D-BCC (42.35%)	30.21	17.61	10.97	13.12	28.09
H-0.875[b]	Designed	17.95	20.51	20.51	20.51	20.51
	Overall	17.33	21.15	20.93	20.18	20.43
	W-FCC (37.12%)	7.99	22.98	27.18	26.10	15.74
	BCC (62.88%)	27.25	18.69	13.43	14.46	26.18
H-1.00[b]	Designed	20.00	20.00	20.00	20.00	20.00
	Overall	20.12	19.58	20.70	20.33	19.27
	W-FCC (18.87%)	6.98	23.12	27.78	27.70	14.42
	BCC (81.13%)	26.49	19.56	12.76	15.52	25.67
H-1.25	Designed	23.81	19.05	19.05	19.05	19.05
	Overall	25.53	19.24	19.06	19.11	19.06
	W-BCC (26.08%)	11.74	18.40	33.63	26.37	9.85
	BCC (matrix, 73.92%)	27.69	19.27	14.32	16.45	22.27
H-1.50	Designed	27.27	18.18	18.18	18.18	18.18
	Overall	27.44	18.69	18.26	17.95	17.66
	W-BCC (18.21%)	11.32	15.68	38.48	27.50	7.02
	BCC (matrix, 81.79%)	31.03	19.07	13.34	15.07	21.49
H-2.00	Designed	33.33	16.67	16.67	16.67	16.67
	Overall	30.13	17.65	17.96	17.29	16.97
	W-BCC (30.94%)	18.19	12.27	36.80	25.21	7.53
	BCC (matrix, 69.06%)	35.48	19.29	10.63	14.21	20.40

[a] *Note*: N, D, and W denote needle-, droplet-, and wall-shaped, respectively. The volume fractions of FCC and BCC phases in the transition region calculated by hardness information shown in Fig. 6 and by Eq. (1).
[b] Duplex structure is shown, where volume fractions for FCC and BCC are shown in parentheses.

the power of 4 as shown in the fitting Eqs. (2) and (3).

$$Y = 0.65X_m^3 + 0.17, \quad (2)$$

$$Y = 429.34X_a^4 + 0.19, \quad (3)$$

where Y is the volume fraction of BCC, X_m is the molar ratio of Al, and X_a is the atomic percent of Al.

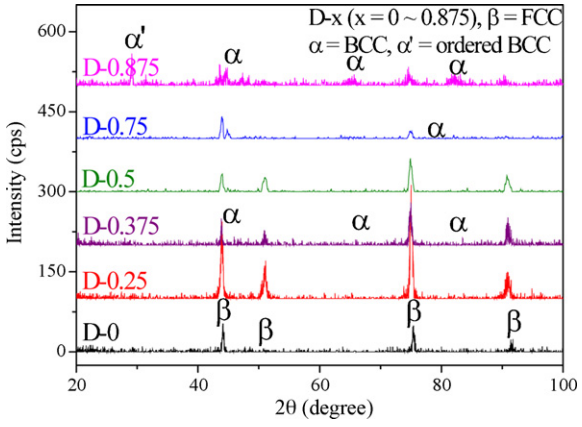

Fig. 7. XRD patterns of D-*x* ($0 \le x \le 0.875$) showing lower intensity than that of H-*x*.

However, it was difficult for the two coexisted BCC phases ($x \ge 1.25$) to calculate their volume fractions. The volume fraction from EDS is a rough estimate. The overall Al at%, Al_{total}, is the sum of both the Al at% of BCC phases, $Al_{BCC(matrix)}$ and $Al_{BCC(wall)}$. The results for H-1.25 to H-2.00 are calculated by Eq. (4) and listed in Table 3.

$$Al_{total} = xAl_{BCC(matrix)} + (1-x)Al_{BCC(wall)}, \quad (4)$$

Table 4
Lattice constants and hardness of H-*x*.

Sample	Lattice constant (Å)		Hardness (Hv)
	FCC phase	BCC phase	
H-0	3.561	–	113.0 ± 0.4
H-0.25	3.573	–	113.0 ± 4
H-0.375[b]	3.569	N/A[a]	196.0 ± 2
H-0.50[b]	3.591	2.873	209.0 ± 12
H-0.75[b]	3.589	2.873	280.0 ± 3
H-0.875[b]	3.577	2.869	361.0 ± 7
H-1.00[b]	3.583	2.862	433.0 ± 22
H-1.25	–	2.866	499.0 ± 23
H-1.50	–	2.871	517.3 ± 21
H-2.00	–	2.866	512.4 ± 18

[a] N/A means "not available".
[b] Shows the FCC–BCC transition region.

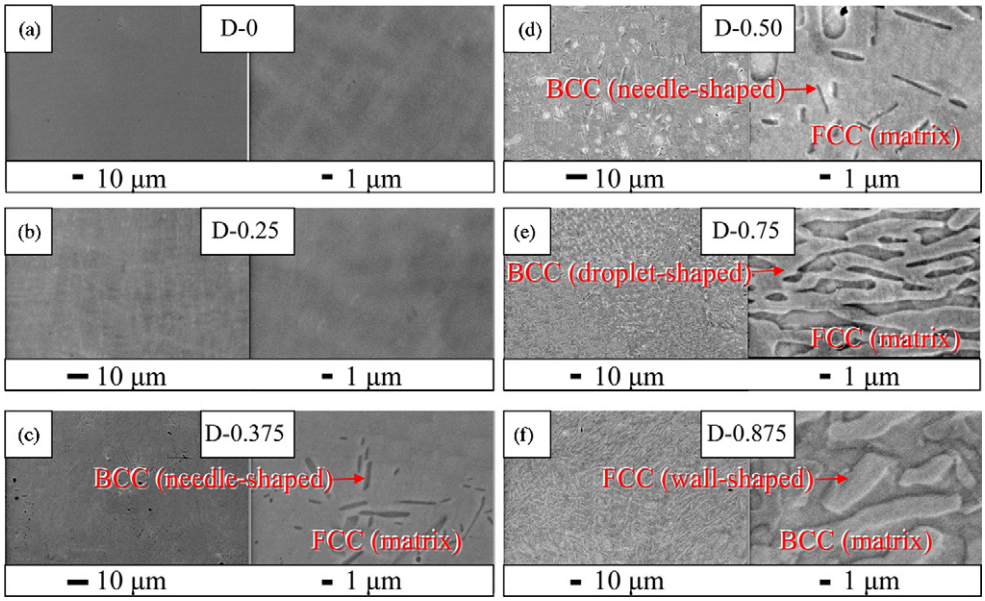

Fig. 8. SEM images for not etched D-*x* samples with lower (left) and higher (right) magnifications.

3.3. As-deformed $Al_xCoCrFeNi$ (D-*x*)

The samples of H-*x* (*x* = 0, 0.25, 0.375, 0.50, 0.75, and 0.875) further deformed by rolling to 50% reduction in thickness are called D-*x*. Rolling is used in this study to induce numerous defects, such as dislocations and lattice distortion. Accordingly, the intensity of the XRD patterns shown in Fig. 7 drastically decrease to 300 cps at least. The corresponding lattice constants are listed in Table 5. However, SEM images shown in Fig. 8 and the EDS compositional analysis shown in Table 6 are almost identical to those of H-*x*.

Note that the volume fractions of FCC and BCC of D-*x* here are assumed to be identical to the counterparts of H-*x*, i.e., no phase transformation occurs during 50%-cold rolling. The hardness of D-*x* showing obvious deformation hardening effect is illustrated and compared with those of H-*x* in Fig. 9(a) and the detailed values and

Table 5
Lattice constants, hardness and hardening ratio for D-*x*.

Sample	Lattice constant (Å)		Hardness (Hv)	Hardening ratio, HR
	FCC phase	BCC phase		
D-0	3.554	–	325 ± 9	1.9
D-0.25	3.578	–	346 ± 5	2.1
D-0.375[b]	3.579	N/A[a]	360 ± 7	0.8
D-0.50[b]	3.561	2.852	368 ± 4	0.8
D-0.75[b]	3.568	2.857	434 ± 8	0.6
D-0.875[b]	3.597	2.856	497 ± 7	0.4

[a] N/A means "not available". Gray area shows the transition region.
[b] Shows the FCC–BCC transition region.

Table 6
EDS analyses (at%) for D-*x*.[a]

Samples	Items	Al (%)	Co (%)	Cr (%)	Fe (%)	Ni (%)
D-0	Designed	0	25.00	25.00	25.00	25.00
	Overall (FCC)	0	25.61	25.17	24.84	24.38
D-0.25	Designed	5.88	23.53	23.53	23.53	23.53
	Overall (FCC)	5.41	23.55	24.17	23.81	23.06
D-0.375[b]	Designed	8.57	22.86	22.86	22.86	22.86
	Overall	7.83	23.03	23.24	22.99	22.91
	FCC (78.85%)	7.08	23.67	23.66	22.98	22.61
	N-BCC (21.15%)	24.93	16.52	11.42	13.52	33.62
D-0.50[b]	Designed	11.11	22.22	22.22	22.22	22.22
	Overall	11.05	21.75	22.86	22.27	22.06
	FCC (75.51%)	7.66	23.12	24.95	23.79	20.48
	N-BCC (24.49%)	29.64	16.47	8.49	11.78	33.61
D-0.75[b]	Designed	15.79	21.05	21.05	21.05	21.05
	Overall	15.45	21.06	21.50	20.99	20.99
	FCC (57.65%)	7.81	22.88	27.80	24.52	16.99
	D-BCC (42.35%)	29.05	17.60	11.00	12.87	29.48
D-0.875[b]	Designed	17.95	20.51	20.51	20.51	20.51
	Overall	16.90	19.77	21.35	20.77	21.22
	W-FCC (37.12%)	6.35	29.37	25.93	22.33	16.02
	BCC (62.88%)	26.87	12.97	15.01	18.30	26.85

[a] Volume fractions of phases are shown in the parentheses. N, D, and W denote needle-, droplet-, and wall-shaped phases, respectively.
[b] Shows the FCC–BCC transition region.

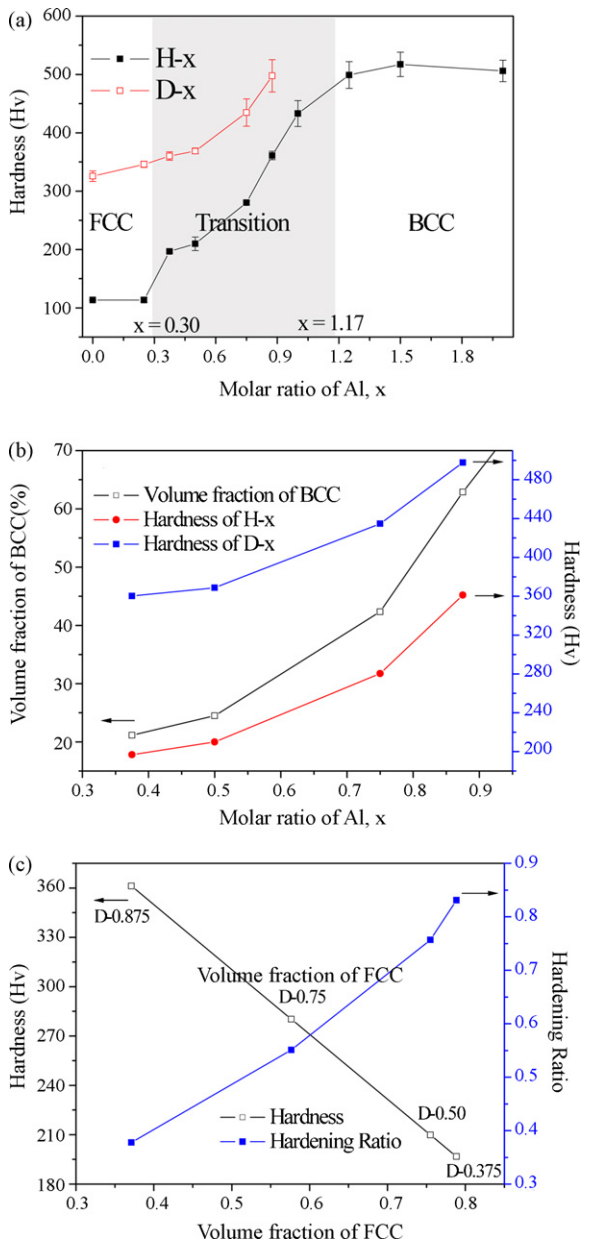

Fig. 9. (a). Plots of hardness for H-x and D-x with error bar. (b) Plots of hardness for H-x and D-x and volume fraction of BCC as a function of the molar ratio of Al, x. Note that the three curves seem to obey the same x dependence in (b). (c) Plots of the hardness and hardening ratio as a function of the volume function of FCC. Note that both curves have monotonically decreasing linear relationship with volume fraction of FCC in (c).

hardening ratio, HR, are listed in Table 5. The hardening ratio, HR, is defined as:

$$\mathrm{HR} = \frac{(H_{\text{D-}x} - H_{\text{H-}x})}{H_{\text{H-}x}}, \tag{5}$$

where the $H_{\text{D-}x}$ and $H_{\text{H-}x}$ are the values of hardness of D-x and H-x, respectively. In Fig. 9(a) and (b), the slope of D-x in the transition region seems to be equal to that of H-x and the curve of volume fraction of BCC. This indicates that the hardness of D-x still relates to the volume fractions of FCC and BCC. Fig. 9(c) demonstrates the monotonically decreasing linear relationship for the hardness and HR to the volume fraction of FCC. This not only explains that the hardness and HR still are simply constituted by the deformation-hardened FCC and BCC but also shows that there are proportional deformation constant among them. Further, for D-x the hardness can be written as follows:

$$H_{\text{D-}x} = (C_{\text{FCC}} H_{\text{H-FCC}}) X_{\text{FCC}} + (C_{\text{BCC}} H_{\text{H-BCC}}) X_{\text{BCC}}, \tag{6}$$

where the C_{FCC} and C_{BCC} are called as the deformation hardening constants, $H_{\text{H-FCC}}$ and $H_{\text{H-BCC}}$ the average hardness values of prior-deformed single FCC and single BCC, X_{FCC} and X_{BCC} the volume fractions of FCC and BCC, respectively. By numerical fitting, the C_{FCC} and C_{BCC} are 2.55 and 1.23, respectively. The result shows the hardening ability of FCC was about twice that of BCC in this high-entropy alloy system. Therefore, the hardness of H-x and D-x obeyed the molar ratio of Al to the power of 2.5–3 in Eq. (3).

4. Conclusions

(1). The structure of as-cast, -homogenized, and -deformed $Al_xCoCrFeNi$ alloys, as the amount x of Al increases, is sequentially single FCC, duplex FCC–BCC, and single BCC. Al is a BCC stabilizer in $Al_xCoCrFeNi$ alloys. The x intervals for existence of duplex phase in as-cast, -homogenized, and -deformed $Al_xCoCrFeNi$ alloys are $0.45 \le x \le 0.88$, $0.30 \le x \le 1.17$, and $0.30 \le x \le 0.875$, respectively.

(2). The compositions for single FCC and single BCC of as-cast alloys, and single FCC of as-homogenized alloys and single FCC of as-50%-rolled alloys are similar to their designed average values.

(3). The duplex FCC–BCC structure in as-homogenized alloys is composed of less Al–Ni FCC and more Al–Ni BCC areas. The interval of amount of Al for duplex phase extends from $0.45 \le x \le 0.88$ for C-x to $0.30 \le x \le 1.17$ for H-x during homogenization. In duplex FCC–BCC of as-homogenized $0.30 \le x \le 0.75$ alloys, the matrix is FCC, while the precipitate is BCC. The morphology of BCC in as-homogenized $0.30 \le x \le 0.75$ alloys, as x increases, is sequentially needle- (N), droplet- (D), and wall-shaped (W). In duplex FCC–BCC of as-homogenized $0.875 \le x \le 1.17$ alloys, the matrix is BCC, while the precipitate is wall-shaped FCC (W-FCC). The single BCC structure in as-homogenized alloys is composed of less Al–Ni wall-shaped ordered BCC (W-BCC) precipitates and more Al–Ni BCC matrix. The as-cast phase is not an equilibrium phase.

(4). The as-deformed $0 \le x \le 0.875$ alloys possess somewhat higher hardness than the as-homogenized $0 \le x \le 0.875$ alloys but with the same microstructure, compositions, and volume fractions of FCC and BCC phases. There is no stress-induced phase transformation during plastic deformation of alloys. The ratio of hardening (HR) after 50%-deformation varies from 0.4 to 2.0 that decreases as the amount of Al increases. The main strengthening mechanism is work hardening.

(5). The hardening ability of FCC was about twice that of BCC in this high-entropy alloy system.

Acknowledgements

The authors gratefully acknowledge financial support from National Science Council of Taiwan (NSC96-2221-E007-066-MY3). One of the authors, SKC, also would express his appreciation to the CSC Group Education Foundation of China Steel Corporation for financial support in this study.

References

[1] G.L. Chen, C.T. Liu, Int. Mater. Rev. 46 (2001) 253–260.
[2] A. Peker, W.L. Johnson, Appl. Phys. Lett. 63 (1993) 2342–2344.
[3] A. Inoue, A. Takeuchi, Mater. Sci. Eng. A375-377 (2004) 16–30.
[4] W.H. Wang, C. Dong, C.H. Shek, Mater. Sci. Eng. R44 (2004) 45–89.
[5] A.L. Greer, Nature 366 (1933) 303–304.
[6] K.H. Huang, A Study on the Multicomponent Alloy Systems Containing Equal-mole Elements, M.S. thesis, Department of Material Science and Engineering, NTHU, Taiwan, 1996.

[7] J.W. Yeh, S.K. Chen, S.J. Lin, J.Y. Gan, T.S. Chin, T.T. Shun, C.H. Tsau, S.Y. Chang, Adv. Eng. Mater. 6 (2004) 299–303.
[8] C.J. Tong, Y.L. Chen, S.K. Chen, J.W. Yeh, T.T. Shun, C.H. Tsau, S.J. Lin, S.Y. Chang, Metal. Mater. Trans. A36 (2005) 881–893.
[9] Y.J. Zhou, Y. Zhang, Y.L. Wang, G.L. Chen, Appl. Phys. Lett. 90 (2007) 181904.
[10] Y.Y. Chen, U.T. Hong, H.C. Shih, J.W. Yeh, T. Duval, Corros. Sci. 47 (2005) 2679–2699.
[11] H.P. Chou, Y.S. Chang, S.K. Chen, J.W. Yeh, Mater. Sci. Eng. B163 (2009) 184–189.
[12] J.W. Yeh, S.J. Lin, T.S. Chin, J.Y. Gan, S.K. Chen, T.T. Shun, C.H. Tsau, S.Y. Chou, Adv. Eng. Mater. 6 (2004) 74–78.
[13] C.J. Tong, Y.L. Chen, S.K. Chen, J.W. Yeh, T.T. Shun, C.H. Tsai, S.J. Lin, S.Y. Chang, Metal. Mater. Trans. A36 (2005) 881–893.
[14] J.W. Yeh, Ann. Chim. Sci. Mater. 31 (2006) 633–648.
[15] T.K. Chen, M.S. Wong, T.T. Shun, J.W. Yeh, Surf. Coat. Technol. 200 (2005) 1361–1365.
[16] Y.Y. Chen, U.T. Hong, J.W. Yeh, H.C. Shih, Appl. Phys. Lett. 87 (2005) 261918.
[17] Y.Y. Chen, U.T. Hong, J.W. Yeh, H.C. Shih, Scripta Mater. 54 (2006) 1997–2001.
[18] H.F. Kuo, W. Chin, T.W. Cheng, W.K. Hsu, J.W. Yeh, Appl. Phys. Lett. 89 (2006) 182503.
[19] C.H. Lai, S.J. Lin, J.W. Yeh, S.Y. Chang, Surf. Coat. Technol. 201 (2006) 3275–3280.
[20] C.C. Tung, J.W. Yeh, T.T. Shun, S.K. Chen, Y.S. Huang, H.C. Chen, Mater. Lett. 61 (2007) 1–5.
[21] X.F. Wang, Y. Zhang, Y. Qiao, G.L. Chen, Intermetallics 15 (2007) 357–362.
[22] M.H. Tsai, C.W. Wang, C.H. Lai, J.W. Yeh, J.Y. Gan, Appl. Phys. Lett. 92 (2008) 052109.
[23] Y.P. Wang, B.S. Li, M.X. Ren, C. Yang, H.Z. Fu, Mater. Sci. Eng. A491 (2008) 154–158.
[24] See, for example B.D. Cullity, Elements of X-ray Diffraction, 2nd ed., Addison-Wesley, Reading, Massachusetts, 1978 (Fig. 11-4, p. 356).
[25] C.P. Lee, C.C. Chang, Y.Y. Chen, J.W. Yeh, H.C. Shih, Corros. Sci. 50 (2008) 2053–2060.
[26] B.D. Cullity, Introduction to Magnetic Materials, Addison-Wesley, Reading, Massachusetts, 1972.